Scalable Ultrasmall Three-Dimensional Nanowire Transistor Probes for Intracellular Recording

Supplementary Information

Scalable ultrasmall three-dimensional nanowire transistor probes for intracellular recording

Yunlong Zhao, Siheng Sean You, Anqi Zhang, Jae-Hyun Lee, Jinlin Huang and Charles M. Lieber

This file contains:

Supplementary Figures 1 – 16

Supplementary Table 1 – 4

Supplementary References

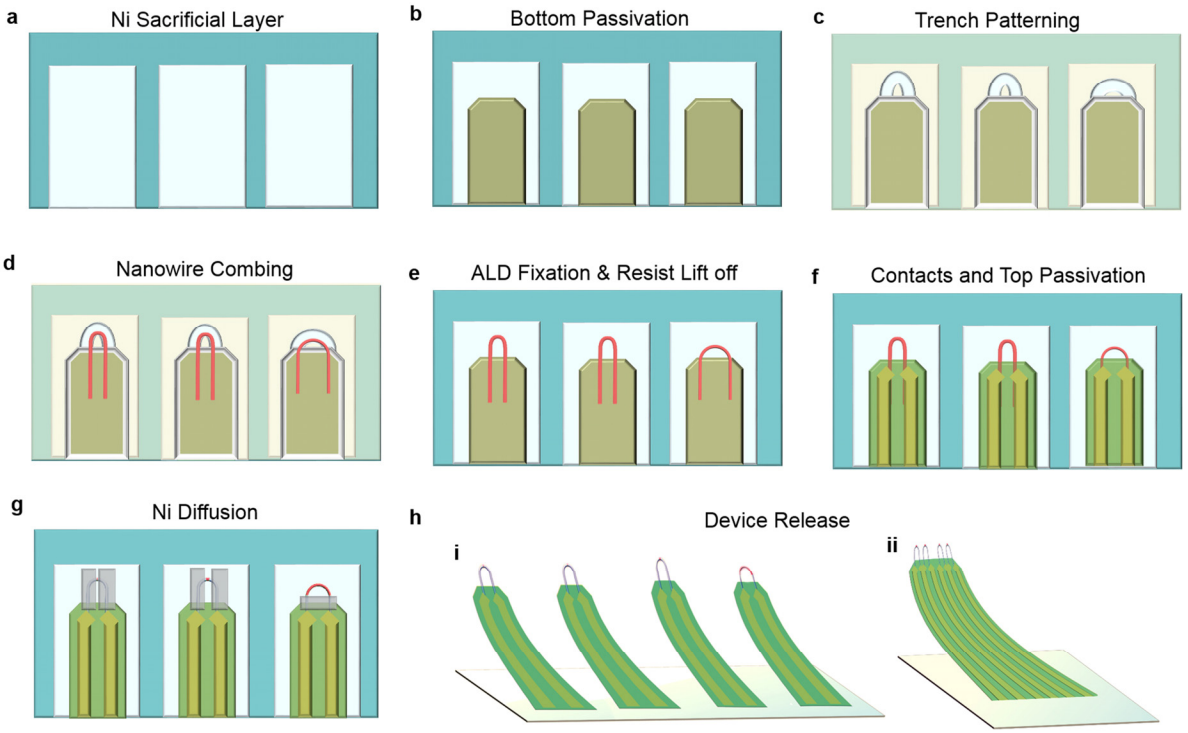

Supplementary Figure 1 | Schematic representation of fabrication of U-shaped nanowire field effect transistor probes. a, Patterning and deposition of Ni sacrificial layer (light cyan, 60nm). **b**, Patterning and deposition of bottom Si_3N_4 passivation layer (tan, 60nm). **c**, Patterning of U-shaped trenches (light cyan) on photoresist (light yellow). **d**, Shape-controlled deterministic nanowire assembly. **e**, Deposition of Al_2O_3 (ca. 1.4 Å) by ALD to fix nanowire position and subsequent removal of photoresist during liftoff step. **f,** Patterning and deposition of asymmetrically strained interconnects Cr/Au/Cr (khaki,1.5/60/60 nm) and top Si_3N_4 passivation layer (yellow green, 60nm). **g**, Patterning and deposition of Ni diffusion layer (light grey, 20nm), lift-off, and rapid thermal annealing to selectively transform the Si nanowire segments underneath and adjacent to the Ni diffusion layer to NiSi. **h**, Removal of Ni sacrificial and diffusion layers by Ni etchant to allow the release of (**i**) single U-NWFET probes or (**ii**) up to 4 U-NWFETs probes per bend-up arm.

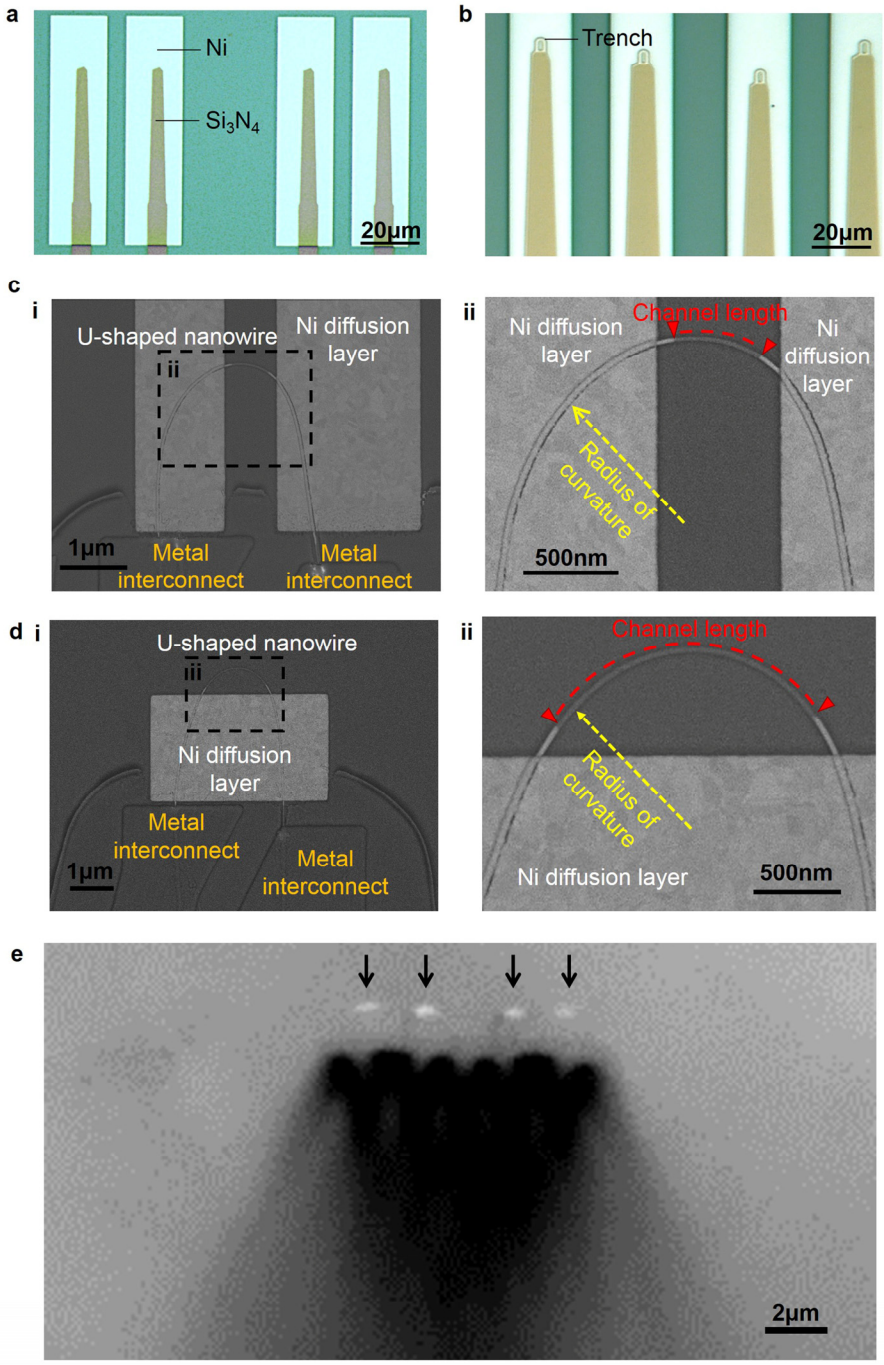

Supplementary Figure 2 | Optical/SEM images of intermediate steps in U-shaped nanowire field effect transistor probe fabrication. a, Optical image showing the bottom Si_3N_4 layer on predefined Ni sacrificial layer. **b**, Optical image showing the U-shaped trenches in front of bottom Si_3N_4 layer. **c,** SEM image showing U-NWFET with ca. 500 nm channel length following nickel diffusion and prior to device release. (**i**) SEM image showing U-shaped nanowire, Ni diffusion layer and metal interconnects. (**ii**) SEM image of the dashed region in **c**(**i**) showing Si and NiSi segments on the U-NWFET tip after annealing **d,**

SEM image showing U-NWFET with ca. 2000 nm channel length following nickel diffusion and prior to device release. (**i**) SEM image showing U-shaped nanowire, Ni diffusion layer and metal interconnects. (**ii**) SEM image of the dashed region in **d**(**i**) showing the Si and NiSi segments on the U-NWFET tip after annealing. In panels c and d, red arrows and dashed lines designate the FET channel length, and yellow arrows and dashed lines designate the radius of curvature (ROC). **e**, Optical image of 4 U-NWFETs probes on one bend-up arm. Here the arrows show the position of each U-NWFETs.

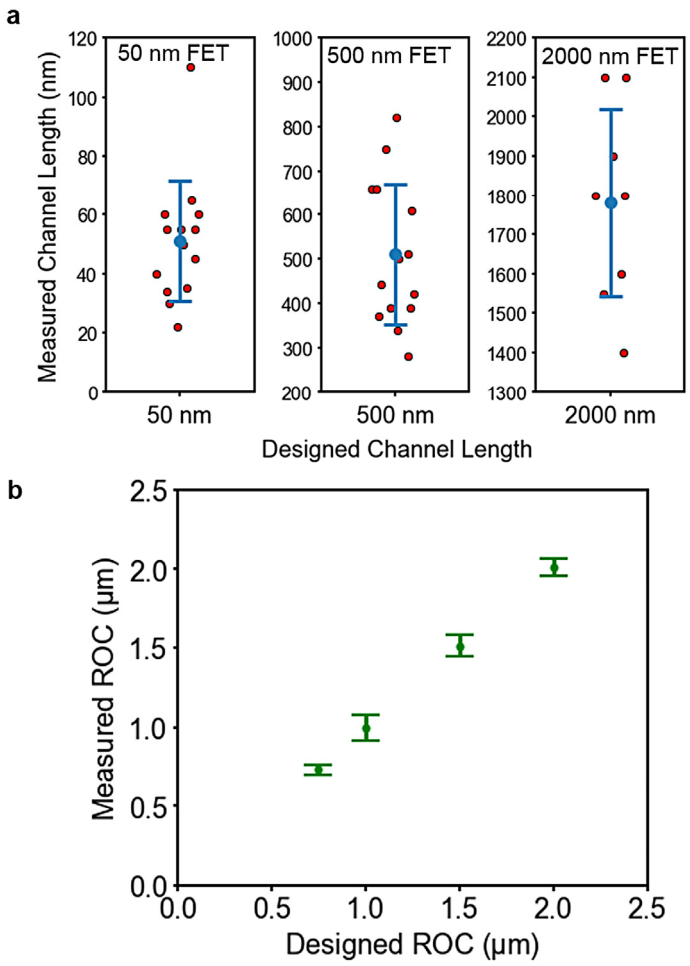

Supplementary Figure 3 | Characterization of the variation in U-shaped nanowire field effect transistor channel length and radii of curvature following device fabrication. a, Plot showing distribution of channel lengths measured using SEM versus designed channel lengths: 50, 500 and 2000 nm. The average and standard deviation values are 51 ± 21 nm (N=14), 510 ± 170 nm (N=14) and 1780 ± 250 nm (N=8) for designed channel lengths of 50, 500 and 2000 nm respectively. Red dots are values for individual devices while the blue dots and error bars represent the mean and standard deviation respectively. **b**, Plot comparing mean and standard deviation of measured ROC with the designed nanowire ROC. The average and standard deviation values are 710 ± 30 nm (N=8), 1060 ± 90 nm (N=8), 1510 ± 70 nm (N=5), and 2010 ± 60 nm (N=5) for designed ROC of 0.75, 1.0, 1.5 and 2.0 μm respectively. All the error bars reflect ±1 s.e.m.

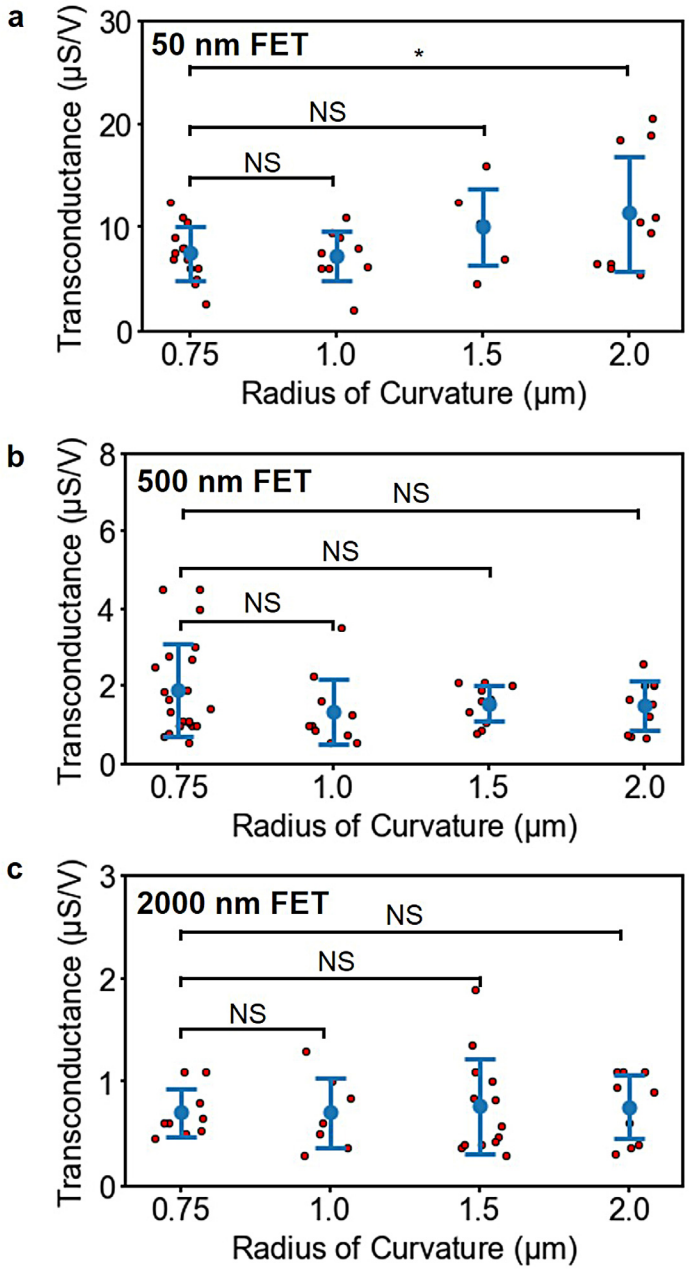

Supplementary Figure 4 | Transconductance versus radii of curvature for U-shaped nanowire field effect transistor probes with fixed channel length of ca. (a) 50 nm, (b) 500 nm and (c) 2000 nm FET. Red dots indicate individual devices, while the larger blue dot with bars show the average and standard deviation of transconductance for each ROC. The p-values shown above were obtained by comparing the datasets below the ends of the black line using the student's t test (See specific statistics in **Supplementary Table 1**). NS: not significant, p-value > 0.05; *: 0.01< p-value < 0.05. These data show that there are no statistically-significant differences in the transconductance as a function of the designed ROC for fixed channel lengths of 500 nm and 2000 nm. For fixed channel length of 50 nm, a statistically significant

difference in transconductance was observed only when comparing between devices with ROC of 0.75 μm and 2.0 μm. All the error bars reflect ±1 s.e.m.

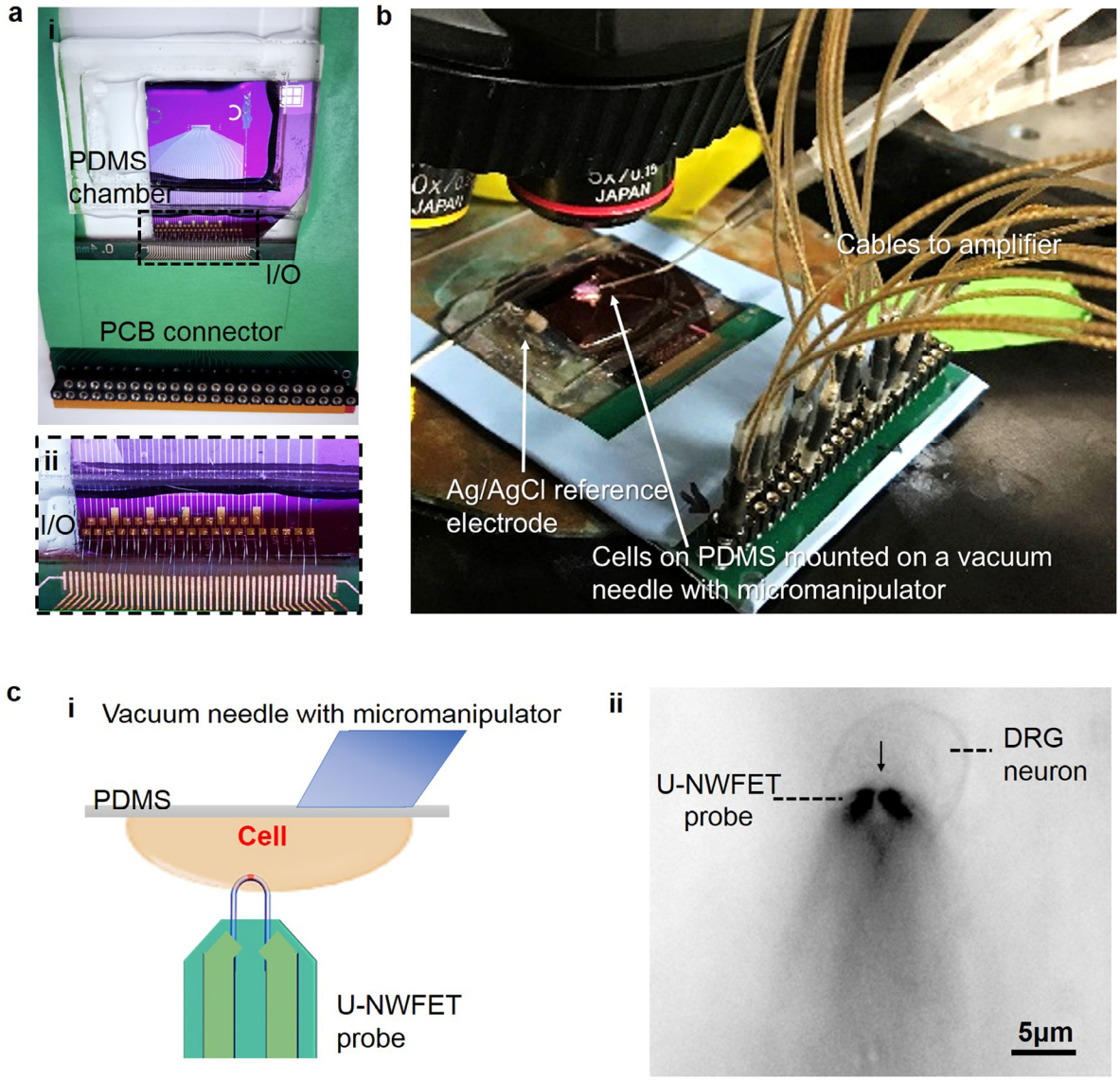

Supplementary Figure 5 | Electrical input/output (I/O) of devices, cell measurement set-up and probe/cell interface. a, Photograph of PCB connector attached adjacent to the I/O region of devices; (**i**) Overview image of assembled device with mounted measurement chamber (**ii**) Zoom-in image of area marked by dashed lines in (i) showing wire bonding between PCB board and I/O region. **b**, Photograph of the cell measurement set-up, with pin connectors leading to amplifier, refence electrode in the measurement chamber, and vacuum needle holding PDMS with cultured cells under an optical microscope. **c**. Schematic and optical image of probe/cell interface; (**i**) Side view schematic of the probe/cell; (**ii**) Top view optical image of probe/cell, showing single U-NWFET probe recording from one DRG neuron cultured on PDMS. The arrow shows the position of the U-NWFET.

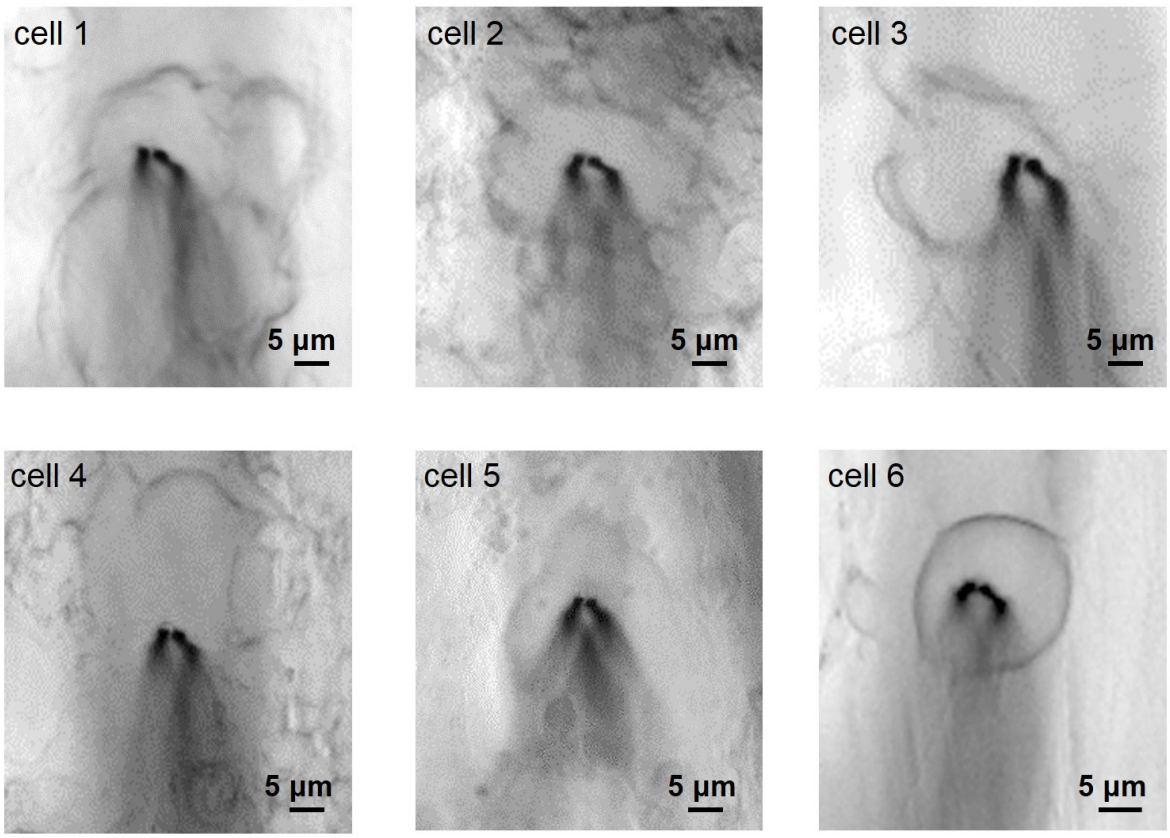

Supplementary Figure 6 | Optical images of the same U-shaped nanowire field effect transistor device interfaced to cells 1-6 shown in Fig. 3a.

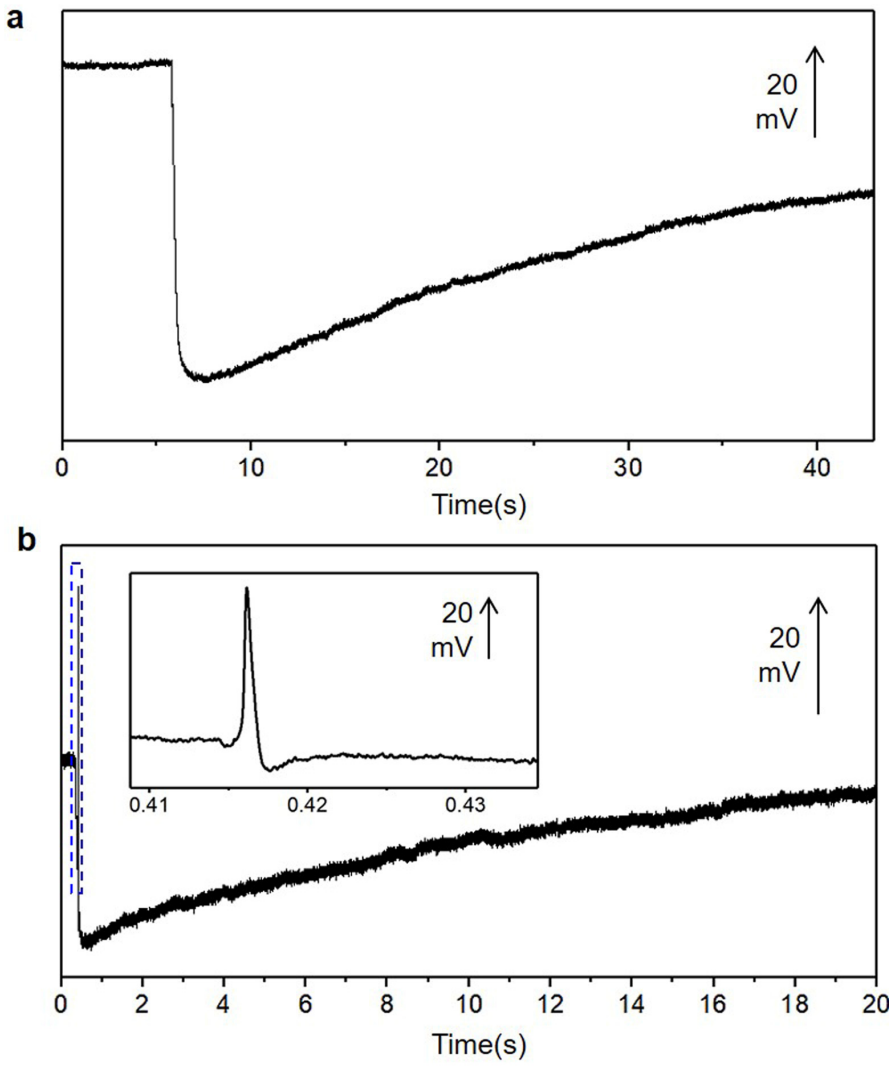

Supplementary Figure 7 | Additional examples of intracellular recording from DRG neurons without spontaneous firing properties. a, Intracellular recording from a neuron with a voltage drop upon contact with the probe, likely due to the negative resting membrane potential. **b,** Intracellular recording from a neuron that shows one action potential followed by a voltage drop upon contact with the probe. Inset shows the zoom-in view of the highlighted action potential spike.

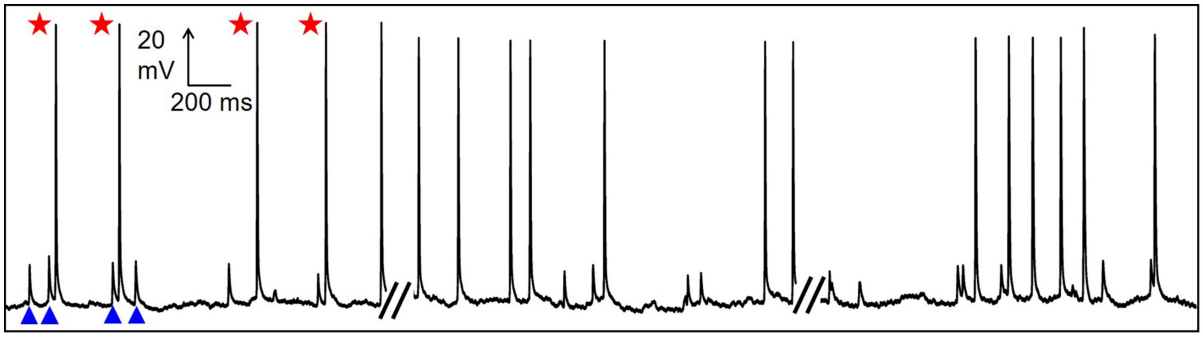

Supplementary Figure 8 | Representative patch clamp recording of a spontaneously firing DRG cell. This cell exhibits both action potentials (highlighted by red stars) and subthreshold activity (highlighted by blue triangles).

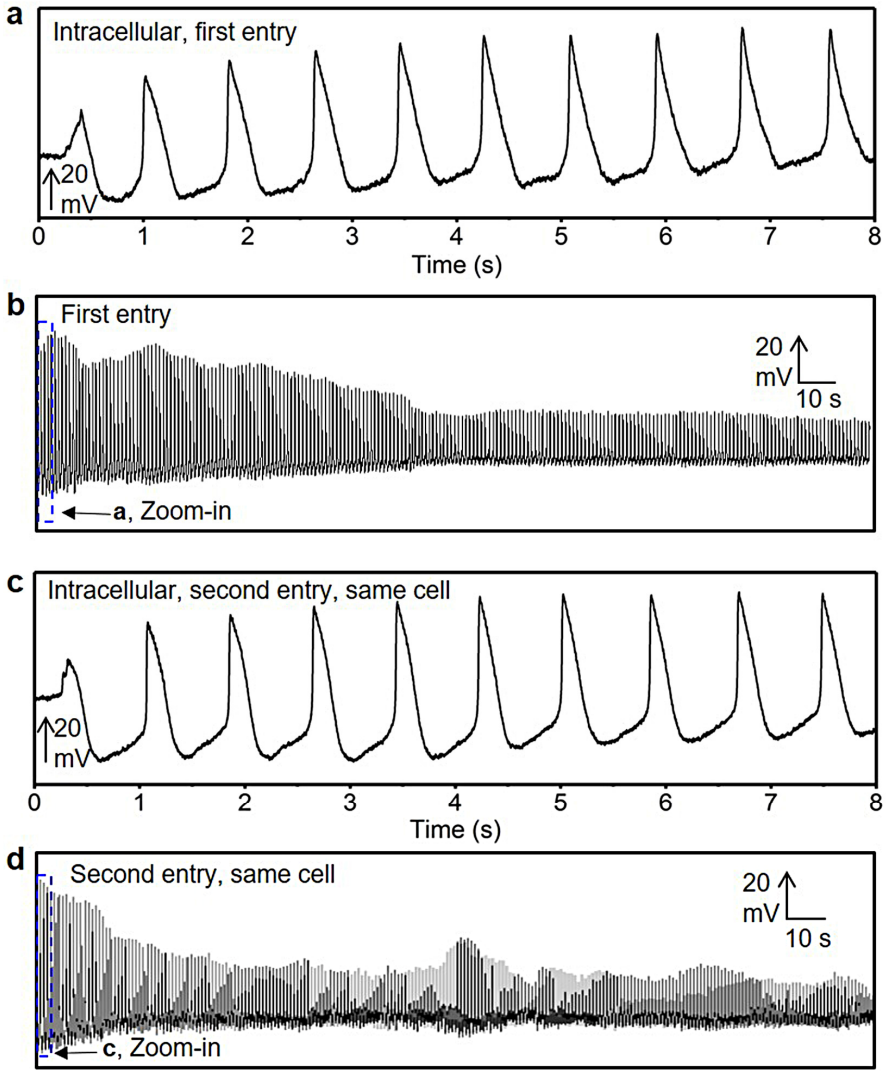

Supplementary Figure 9 | Repeated intracellular recording from one HiPSC-CM by one U-shaped nanowire field effect transistor probe with 50 nm channel length and 0.75µm radii of curvature. a, Initial entry and intracellular recording of HiPSC-CM using a U-NWFET. **b**, ca. 3 min trace of the first entry and intracellular recording with 0.4 Hz high pass filter. The portion of the trace shown in **a** is marked by dashed blue lines. The action potential frequency of first recording is 1.25 ± 0.04 Hz. During the ca. 3-minute recording, there is a gradual decrease in the peak amplitude to 20 mV and an ca. 10 mV increase in baseline, although it remains relatively stable at the latter value for 2 min. **c**. Second intracellular entry and recording using the same U-NWFET on the same cell. After the initial recording, the cell was separated from the U-NWFET for several minutes, and then brought back into the same z position without changing the x/y position on the micromanipulator or the probe position. **d**. ca. 3 min trace of the second entry and intracellular recording with 0.4 Hz high pass filter, which is similar to that used by other groups [S1-S3]. The portion of the trace shown in **c** is marked by dashed blue lines. The action potential frequency of the second recording is 1.23 ± 0.02 Hz, which is comparable to the first recording, suggesting that U-NWFET probe penetration does not affect cell viability and is minimally invasive.

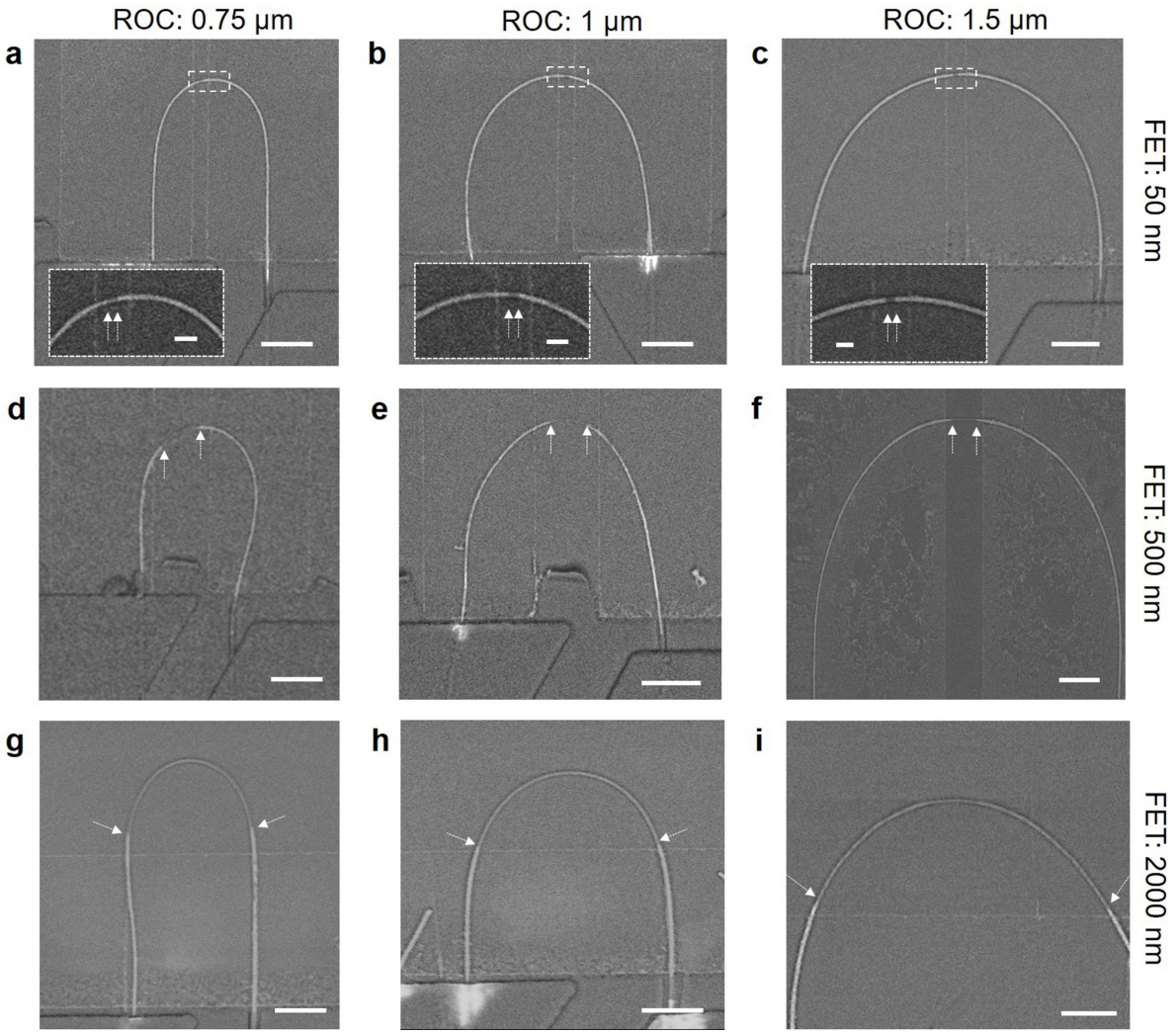

Supplementary Figure 10 | SEM images of U-shaped nanowire field effect transistors with varied channel lengths and radii of curvature. a-c, ca. 50 nm FET with ROC of (**a**) ca. 0.75 µm, (**b**) ca. 1 µm and (**c**) ca. 1.5 µm. Insets are the zoom-in view the U-NW tip; all scale bars in insets are 100 nm. **d-f**, ca. 500 nm FET with ROC of (**d**) ca. 0.75 µm, (**e**) ca. 1 µm and (**f**) ca. 1.5 µm. **g-i**, ca. 2000 nm FET with ROC of (**g**) ca. 0.75 µm, (**h**) ca. 1 µm and (**i**) ca. 1.5 µm. White arrows indicate the transition points between Si and NiSi on the NW. All scale bars except those in insets are 500 nm. Devices fabricated for SEM imaging did not have a bottom Ni sacrificial layer to improve contrast during imaging.

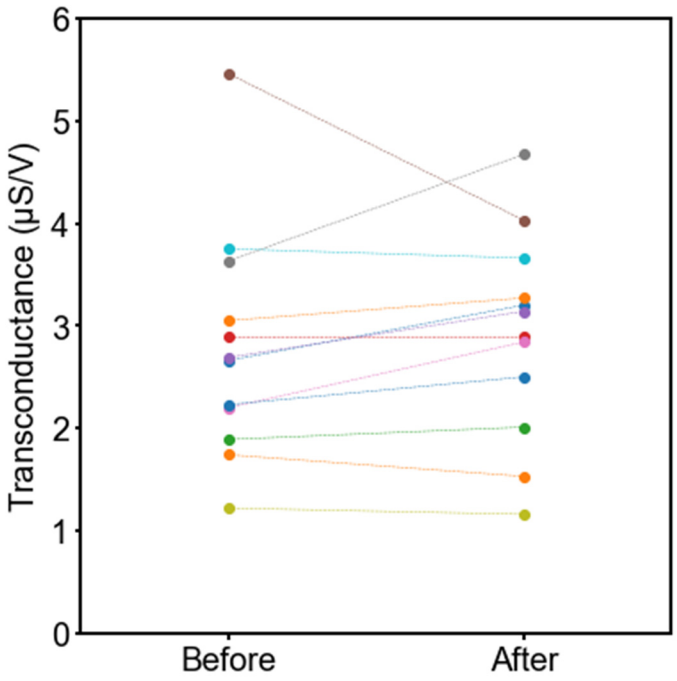

Supplementary Figure 11 | Transconductance for 10 representative devices before and after ca. 1.5 hr cell measurements. Different colors denote individual devices and the dashed lines are guides between the before and after measurements for each individual device.

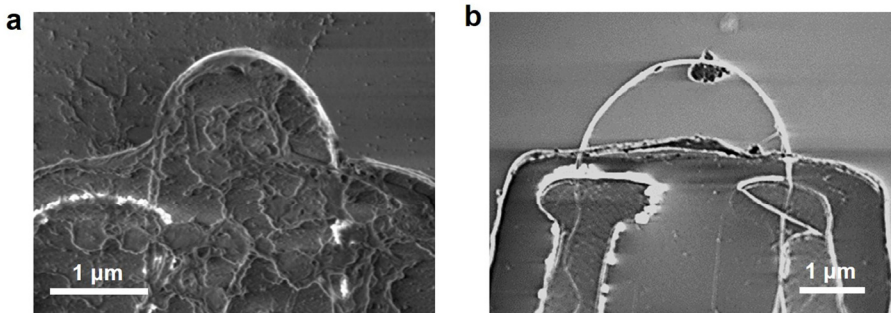

Supplementary Figure 12 | SEM images of devices following recording measurements and removal from cells and solution. **a**, ROC 0.75 µm; **b**, ROC 1.5 µm. In both images, the ROC and U-shape is maintained following measurements. Additional materials on the nanowire are likely cell membrane components that accumulate over multiple intracellular measurements. Optical images (Supplementary Fig. 6) of the device-cell interface for six different cells with the same U-NWFET, transconductance device data (Supplementary Fig. 11) recorded before and after cell measurements, and ROC of U-NWFET devices (Supplementary Fig. 12) measured by SEM following the cell measurements are all constant ROC and stable devices.

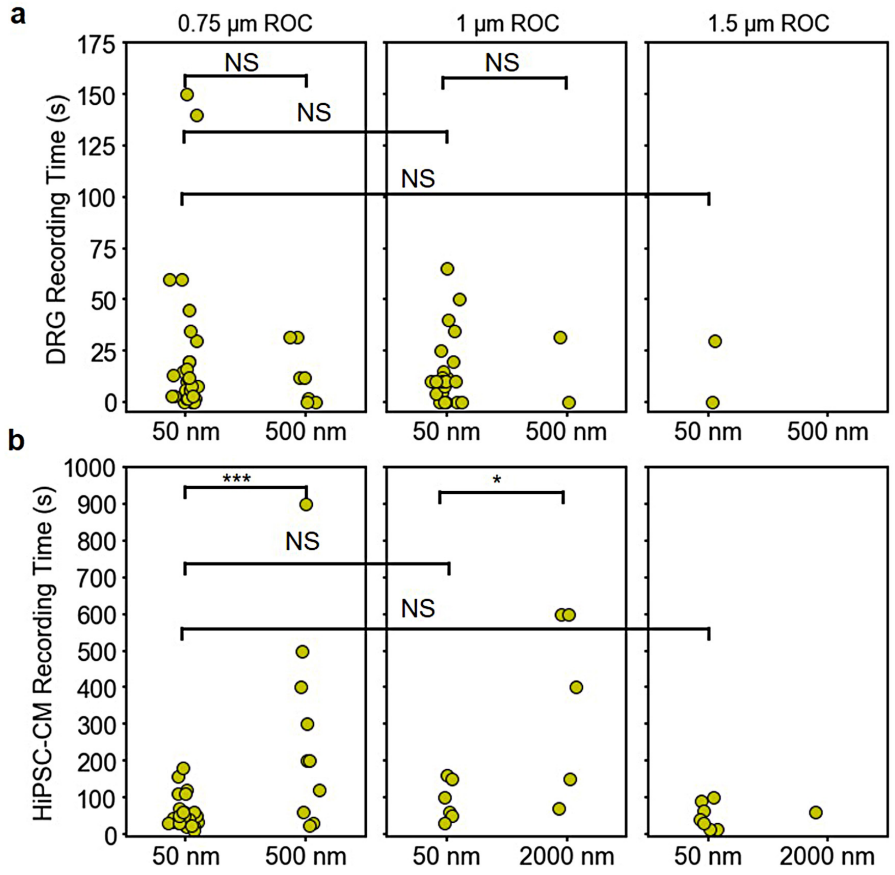

Supplementary Figure 13 | Duration of each recording as separated by radii of curvature and channel length. a, DRG; **b**, HiPSC-CM. There are no significant differences in recording duration with increasing ROC. Additionally, increasing channel length showed no statistically significant difference in the DRG cells, while for the HiPSC-CM, increasing channel length was correlated with an increase in recording duration. ***: p-value < 0.001. See specific statistics in **Supplementary Table 4**.

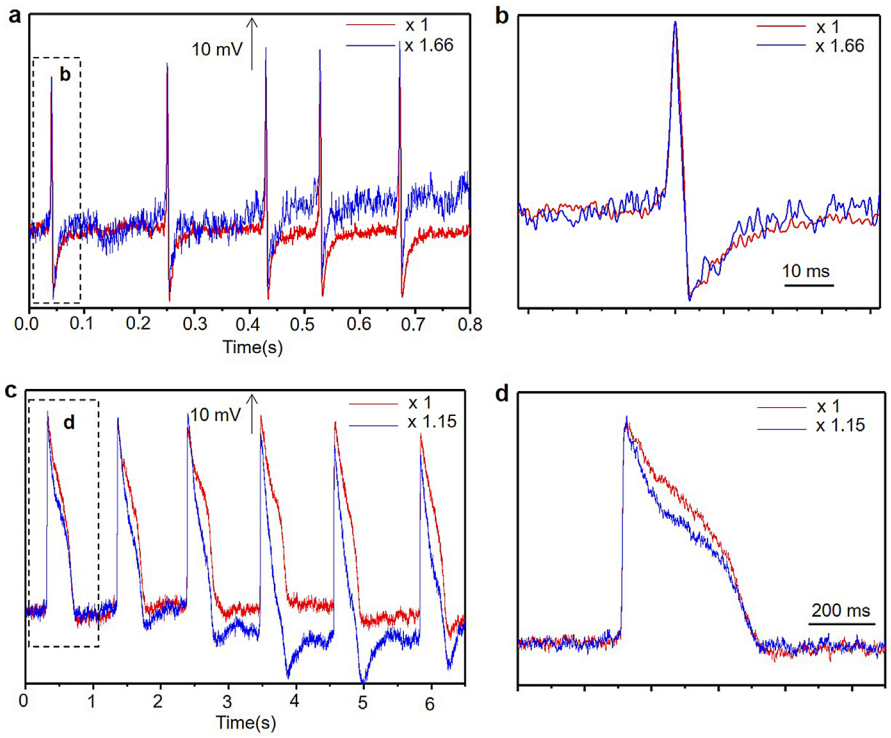

Supplementary Figure 14 | Overlap of scaled action potential waveforms recorded from the same cell by paired U-shaped nanowire field effect transistors on one probe arm. a, Overlap of traces of paired measurements on DRG neurons shown in Fig. 5b. **b,** Zoom-in view of selected peak in **a**. **c,** Overlap of traces of paired measurements on HiPSC-CM shown in Fig. 5c,i. **d,** Zoom-in view of selected peak in **c**. Comparison of the waveform of the cardiomyocyte action potential peaks recorded by the two paired channels indicate close overlap in the depolarization phase, but slight differences in the repolarization phase. These differences occur during the contraction of the cardiac cells associated with the Ca^{2+} flows during the repolarization[S4]. The legends denote the scaling factor used to visually compare the data recorded by the two independent devices in each cell.

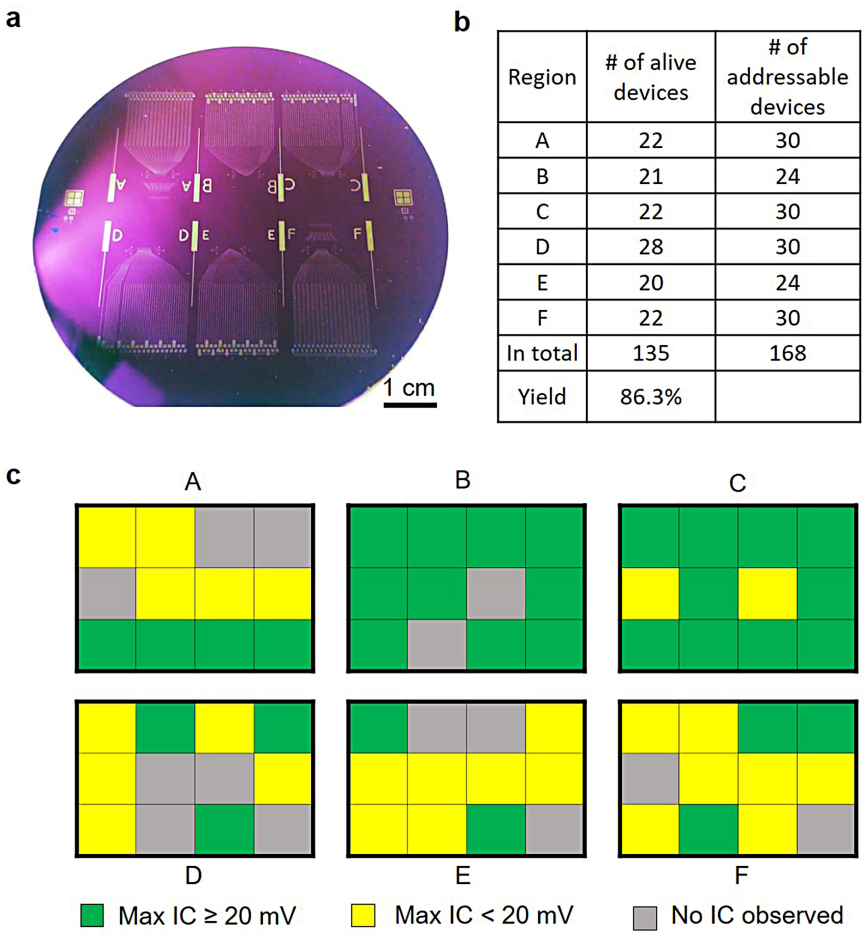

Region	# of alive devices	# of addressable devices
A	22	30
B	21	24
C	22	30
D	28	30
E	20	24
F	22	30
In total	135	168
Yield	86.3%	

Supplementary Figure 15 | Optical image, statistics of devices and mapping of intracellular signal amplitudes from device arrays fabricated on one 76 mm wafer. a, Image of U-NWFET wafer following scalable fabrication process with 6 separate device regions A-F, prior to wafer dicing and wire bonding. **b,** Table indicating number of conductive devices in all addressable device sites following fabrication process and device release. Regions A, C, D, F with 30 channels contains single U-NWFETs while regions B, E with 24 addressed devices were designed with multi U-NWFET probes. For each region/wafer piece, 12 devices were selected and connected to measurement system for cell measurements. **c,** Device map showing the intracellular signal amplitudes recorded by the 12 connected devices for each region from a sheet of HiPSC-CM in separate measurements.

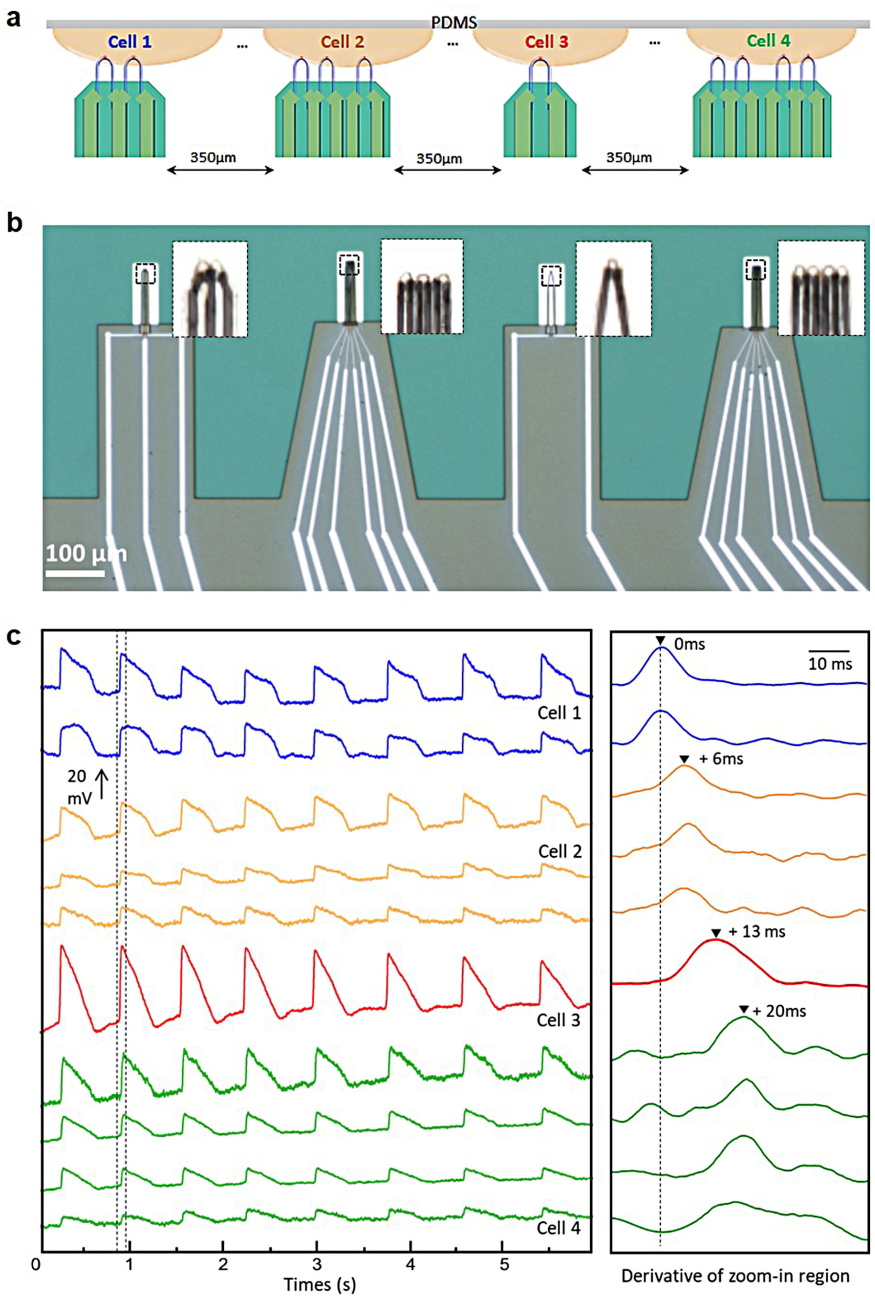

Supplementary Figure 16 | Multiplexed electrophysiological recording by 10 U-shaped nanowire field effect transistors on four probe arms. a, Schematic showing simultaneous recording from a sheet of HiPSC-CM using four probes with 1-4 U-NWFETs per bend probe up arm. U-NWFETs on each bend up probe arm have a spacing of ca. 2 μm while the four probe arms are each separated by 350 μm. Insets show zoom-in views of the highlighted nanowire regions. **b,** Optical image showing device layout prior to Ni etching, with 2, 3, 1 and 4 U-NWFETs for targeting 4 separate cells. **c,** Simultaneous 10 channel recording traces showing characteristic cardiac action potentials in all channels. Traces with matching colors are measured by U-NWFETs on the same bend up probe arm. The vertical dashed guiding line indicates the

time point of the first action potential. An ca. 6-7 ms time delay is observed between probes on any two nearby probe arms, while no discernible delay observed between probes on same probe arm. Those delay time and probe separation yield a signal propagation speed of 5-6 cm/s, which agrees with that reported in the literature for HiPSC-CM in 2D culture[S5].

Supplementary Table 1. Summary statistics for the calculation of t-values, p-values and significance between transconductance versus ROC for U-NWFET devices with fixed FET channel lengths of ca. (a) 50 nm, (b) 500 nm and (c) 2000 nm FET. NS: not significant, p-value > 0.05; *: 0.01< p-value < 0.05. These data show that there are no statistically significant differences in the transconductance as a function of the designed ROC for fixed channel lengths of 500 nm and 2000 nm. For fixed channel length of 50 nm, a statistically significant difference in transconductance was observed only when comparing between devices with ROC of 0.75 μm and 2.0 μm. These results suggest that there is not a strong correlation between ROC and transconductance within the strain regime of our U-NWFET devices.

Device type (ROC/channel length)	Transconductance Comparison		
	t-value	p-value	significance
0.75 μm/50 nm vs 1.0 μm/50 nm	0.234	0.82	NS
0.75 μm/50 nm vs 1.5 μm/50 nm	1.74	0.10	NS
0.75 μm/50 nm vs 2.0 μm/50 nm	2.19	0.039	*
0.75 μm/500 nm vs 1.0 μm/500 nm	1.33	0.19	NS
0.75 μm/500 nm vs 1.5 μm/500 nm	0.87	0.39	NS
0.75 μm/500 nm vs 2.0 μm/500 nm	0.90	0.38	NS
0.75 μm/2000 nm vs 1.0 μm/2000 nm	0.0086	0.99	NS
0.75 μm/2000 nm vs 1.5 μm/2000 nm	0.38	0.71	NS
0.75 μm/2000 nm vs 2.0 μm/2000 nm	0.40	0.69	NS

Supplementary Table 2. Estimated strain versus ROC for U-NWFET devices. The strain in the curved parts of nanowires was calculated by dividing the ROC (0.75, 1, 1.5, 2 μm) by the radius of the nanowire (7.5 nm) [S6]. The relatively low strain (≤1%) in the curved parts of nanowire is consistent with the phenomenon that the transconductance of the device does not vary significantly with the change in ROC (Supplementary Figure 4). Nevertheless, future work investigating reduction in the ROC to below 200 nm could yield strains greater than 3.75 % expected[S6] to show strain-induced enhancements in the transconductance.

Designed ROC (μm)	0.75	1	1.5	2
Strain (%)	1.00	0.75	0.50	0.38

Supplementary Table 3. Statistical analyses of cell measurements with varying radii of curvature and channel lengths. Distributions of recorded amplitudes are compared in this table using the t-test with t-values and p-values calculated using the ttest_ind function from the scipy.stats software package. Unsuccessful recordings were considered as having 0 mV recorded amplitude. A statistically significant difference in the recorded amplitudes is observed in measurements with both DRG neurons and HiPSC-CM when comparing between maximum spike amplitude distributions between different ROC (50 nm FET with 0.75 μm ROC vs 1.0 and 1.5 μm ROC) and channel length (50 nm FET with 0.75 μm ROC vs 500 nm FET with 0.75 μm ROC). ****: p-value < 0.0001. This indicates that decreasing ROC and channel length enables higher amplitude intracellular recordings.

Cell type (ROC/channel length)	Amplitude Comparison			Number of successful intracellular recordings /total recordings
	t value	p-value	significance	
DRG (0.75 μm/50nm vs 1.0 μm/50nm)	2.21	0.031	*	24/30 vs 25/30
DRG (0.75 μm/50 nm to 1.5 μm/50 nm)	5.25	2.15E-06	****	24/30 vs 2/30
HiPSC-CM (0.75 μm/50 nm to 1.0 μm/50 nm)	8.12	3.39E-11	****	31/31 vs 6/30
HiPSC-CM (0.75 μm/50 nm to 1.5 μm/50 nm)	9.53	1.5E-13	****	31/31 vs 7/30
DRG (0.75 μm/50 nm vs 0.75 μm/500 nm)	7.53	3.41E-10	****	24/30 vs 7/30
HiPSC-CM (0.75 μm/50 nm vs 0.75 μm/500 nm)	5.49	9.01E-7	****	31/31 vs 10/30

Supplementary Table 4. Summary statistics for t-values, p-values and significance between the duration of each successful intracellular recording as separated by ROC and FET channel length. For both DRG Neurons and HiPSC-CM, no statistically significant difference was observed in the recording duration obtained with varying ROC. For HiPSC-CM measurements, increasing channel length from 50 nm to 500 nm for the 0.75 μm ROC and from 50 nm to 2000 nm for the 1.0 μm ROC U-NWFET resulted in a statistically significant increase in recording duration. No statistically significant correlation between channel length and ROC was observed for recordings with DRG neurons. We attribute this different to reported difference in cell membrane mechanical properties between DRG neurons and HiPSC-CM, where neuron cell membranes are reported to be less fluid than those of cardiac cells[S7].

Cell type (ROC/channel length)	Recording Duration Comparison		
	t-value	p-value	significance
DRG (0.75 μm/50 nm vs 1.0 μm/50 nm)	0.99	0.33	NS
DRG (0.75 μm/50 nm vs 1.5 μm/50 nm)	0.28	0.78	NS
HiPSC-CM (0.75 μm/50 nm vs 1.0 μm/50 nm)	1.87	0.069	NS
HiPSC-CM (0.75 μm/50 nm vs 1.5 μm/50 nm)	0.35	0.73	NS
DRG (0.75 μm/50 nm vs 0.75 μm/500 nm)	0.66	0.51	NS
DRG (1.0 μm/50 nm vs 1.0 μm/2000 nm)	0.12	0.90	NS
HiPSC-CM (0.75 μm/50 nm vs 0.75 μm/500 nm)	4.43	0.0074	***
HiPSC-CM (1.0 μm/50 nm vs 1.0 μm/2000 nm)	2.65	0.027	*

Supplementary References

S1. Abbott, J. et al. CMOS nanoelectrode array for all-electrical intracellular electrophysiological imaging. *Nature Nanotech.* **12**, 460-466 (2017).

S2. Shmoel, N., et al. Multisite electrophysiological recordings by self-assembled loose-patch-like junctions between cultured hippocampal neurons and mushroom-shaped microelectrodes. *Scientific reports* **6**, 27110 (2016).

S3. Xie, C., et al. Intracellular recording of action potentials by nanopillar electroporation. *Nature Nanotech.* **7**, 185–190 (2012).

S4. Woodcock, E. A., & Matkovich, S. J. Cardiomyocytes structure, function and associated pathologies. *Int. J. Biochem. Cell Biol.* ***37***, 1746-1751 (2005).

S5. Zhu, H.Q. et al. Two dimensional electrophysiological characterization of human pluripotent stem cell-derived cardiomyocyte system. *Sci. Rep.* **7**, 43210 (2017).

S6. Zhao, Y. et al. Shape-controlled deterministic assembly of nanowires. *Nano Lett.* **16**, 2644-2650 (2016).

S7. Dietschy, J. M., & Turley, S. D. Thematic review series: brain Lipids. Cholesterol metabolism in the central nervous system during early development and in the mature animal. *J. Lipid Res* **45**, 1375-1397 (2004).